RSC Advances

PAPER

View Article Online
View Journal | View Issue

Cite this: *RSC Adv.*, 2021, **11**, 26791

Silver/silver halide supported on mesoporous ceria particles and photo-CWPO degradation under visible light for organic compounds in acrylonitrile wastewater

Guozheng Zhao, Qingwei Tan, Changbo Li,* Liyan Shang, Daihang Zhang, Xuanxuan Lu and Feng Qiu

Silver/silver halide supported on ordered mesoporous ceria particles (Ag/AgCl/CeO_2) were rapidly prepared by microwave-assisted soft template method, deposition precipitation method and photoreduction method, using cerium nitrate and silver nitrate as raw materials and block copolymer F127 as a template. The morphology, structure and chemical composition of the catalyst were characterized by XRD, SEM, EDS, TEM, N_2 adsorption–desorption and UV-Vis Drs. Catalytic wet peroxide system assisted with visible light photocatalysis (photo-CWPO) was conducted to investigate the performance of organics degradation by Ag/AgCl/CeO_2 as a catalyst in acrylonitrile wastewater. The results showed that the Ag/AgCl/CeO_2 prepared has an ordered mesoporous structure, Ag and AgCl are formed on the surface of CeO_2, with a specific surface area of 302.6–336.2 $m^2\ g^{-1}$ and the average pore size is 8.04–8.90 nm. There is a strong absorption in the visible region and a band gap of 2.9 eV. The Ag/AgCl/CeO_2 catalyst has higher catalytic performance in the photo-CWPO system than in the CWPO system alone. Ag loading, catalyst and H_2O_2 dosage, and pH value can affect the COD removal. When the concentration of COD in acrylonitrile wastewater was 500 mg L^{-1}, the amount of catalyst was 200 mg, the amount of H_2O_2 (30%) was 8 mL, and the reaction time was 60 min, the COD removal reached 90%.

Received 9th June 2021
Accepted 14th July 2021

DOI: 10.1039/d1ra04465f

rsc.li/rsc-advances

Introduction

As an important chemical raw material, acrylonitrile plays an irreplaceable role in industrial production. However, the wastewater from the production process is toxic and harmful because it contains acrylonitrile, acetonitrile, N-heterocyclic compounds and other organic compounds. At present, the treatment methods of acrylonitrile wastewater in industry mainly include biological method, distillation method, incineration method and catalytic oxidation method.[1,2] Due to the poor biodegradability of –CN group compounds in acrylonitrile wastewater, the effluent COD after biological treatment is very high.[3] Distillation method has poor separation effect for components with similar boiling point and high energy consumption. The cost of incineration is high and the equipment is corroded seriously. The catalysts used in catalytic oxidation process, such as metal salts or metal oxides such as iron, copper and nickel, have low catalytic efficiency and serious dissolution of metal ions.[4,5] The typical representative is Fenton catalytic oxidation process. Since the discovery of Fenton reaction in 1894, Fenton oxidation has been widely used to treat high concentration organic wastewater. However, in the application process, the iron hydroxide sludge is produced becomes secondary pollution.[6] Therefore, researchers turned to heterogeneous systems of transition metal catalysts, such as Cu,[7] Co,[8] Mn,[9] *etc.*, and gradually developed catalytic wet peroxide technology (CWPO) on the basis of Fenton method by replacing Fe^{2+} with solid catalysts.[10–12]

With the in-depth study of CWPO technology, all kinds of coupling technologies continue to emerge, expanding the application scope of CWPO technology. Li *et al.*[13] used Cu–Ni bimetallic oxide as catalyst to degrade quinoline in coal chemical wastewater by MW (microwave)-CWPO, and the degradation rate reached 95%. Hassani *et al.*[14] used US (ultrasound)-CWPO to treat azo dye AO7, and the removal was significantly higher than that of CWPO or ultrasound alone. Munoz *et al.*[15] used ilmenite as catalyst to degrade phenol by UV-CWPO, and the TOC removal of total organic carbon reached 100%. UV-CWPO combined with UV irradiation has faster mineralization rate and higher degradation efficiency than dark reaction process.[16] However, ultraviolet light only accounts for about 5% of the solar radiation energy, while visible light accounts for about 50%. Therefore, the development of visible light catalysts has become a new research hotspot in recent years.[17] Huang *et al.*[18] developed a novel plasma photocatalyst Ag@AgCl which is considered to be a good visible light catalyst. At present, a variety of efficient

Liaoning Petrochemical University, Fushun, Liaoning, 113001, China. E-mail: lnpulcb@126.com

composite photocatalysts have been prepared, such as Ag/AgCl/ZnO,[19] Ag/AgCl/Bi_2MoO_6,[20] Ag/AgCl/TiO_2,[21] AgCl/Ag/In_2O_3,[22] Ag/AgCl/WO_3/g-C_3N_4,[23] Ag/AgCl/$ZnWO_4$,[24] *etc.*

In order to degrade organics in acrylonitrile wastewater more efficiently, a photo-CWPO synergy system with visible light was conducted. Ordered mesoporous Ag/AgCl/CeO_2 catalysts were prepared by microwave-assisted soft template method, deposition precipitation method and photoreduction method. And the structure, morphology and elements of the catalyst were characterized systematically. The catalytic performance of Ag/AgCl/CeO_2 in photo-CWPO system for degradation of refractory organic pollutants in acrylonitrile wastewater was studied. The effects of Ag loading, catalyst, H_2O_2 dosage and pH on COD removal were investigated, and the catalytic mechanism of Ag/AgCl/CeO_2 in photo-CWPO system is preliminarily discussed.

Experimental

Materials and methods

Triblock copolymer F127 ($EO_{106}PO_{70}EO_{106}$, Mav = 12 600), cerium nitrate [$Ce(NO_3)_3 \cdot 6H_2O$], hydrogen peroxide solution (H_2O_2, 30%), silver nitrate ($AgNO_3$), sodium hydroxide (NaOH), all reagents used were analytical grade and purchased from Sinopharm Chemical Reagent Co. Shanghai, China. The wastewater was taken from a acrylonitrile chemical plant, the initial concentration of COD is 1500 mg L^{-1} which expressed the concentration of organic matter in wastewater.

Synthesis methods

Synthesis of CeO_2. 5 mmol $Ce(NO_3)_3 \cdot 6H_2O$ was added into a mixture of 20 mL ethanol and 2 g F127, the pH value was adjusted to 10 by NaOH, the mixture was stirred for 60 min at room temperature, then the mixture was reacted in a microwave reactor at 100 °C for 60 min, the gel was dried in oven at 120 °C for 10 hours, then calcined in muffle furnace at 550 °C for 5 h and finally mesoporous CeO_2 was obtained.

Synthesis of Ag/AgCl/CeO_2. 1 g ordered mesoporous CeO_2 was dispersed in 100 mL deionized water and treated with ultrasound for 30 min at room temperature. Then it was mixed with 0.2 mol L^{-1} $AgNO_3$ and 0.1 mol L^{-1} HCl solution. The mixture were treated with ultrasound for another 10 min and then stirred for 60 min. The suspension was centrifugally filtered, washed and dried at 90 °C in oven for 12 h. Finally, the high pressure sodium lamp was used to irradiate the dried powder for 30 min, so that some Ag^+ in the AgCl particle was reduced to Ag, and the Ag/AgCl/CeO_2 was obtained. According to the different amount of $AgNO_3$ added, they are recorded as Ag/AgCl/CeO_2(x), x = 1, 2 and 4 respectively, indicating that the amount of $AgNO_3$ added is 1 mmol, 2 mmol and 4 mmol respectively.

Synthesis of Ag/CeO_2. Another 2 mmol $AgNO_3$ was added into the mixed solution, then under the same conditions the mesoporous Ag/CeO_2 was obtained.

Catalyst characterization. The D8 advance X-ray diffractometer of Brooke spectroscopic instrument company, Germany, using a radiation source Cu (Kα = 1.54178 nm, 40 kV and 15 mA) with a scanning rate of 10 (°) min^{-1}, continuous scanning mode, wide-angle scanning range is 5–90° and small-angle scanning range is 0.5–8.0°. Autosorb-IQ2-MP automatic physical static analyzer of Cantor instrument company, the liquid nitrogen temperature is 77 K. SU8010 field emission scanning electron microscope of Hitachi company, Japan, with accelerating voltage of 15 kV and working distance of WD = 4 mm, JEM-2100F high resolution transmission electron microscope of Japan Electronics Co., Ltd., accelerating voltage 200 kV. Inductively coupled plasma emission spectra of Optima 8000 produced by Perkin Elmer company, USA, with wavelengths of 160 nm–190 nm. Agilent Cary 5000 UV Vis NIR spectrophotometer, Agilent Technologies, USA.

Catalytic performance test. The waste water in this experiment was the actual wastewater from acrylonitrile production, and the composition of organic pollutants was complex. Therefore, the COD removal indicates the catalytic degradation performance. 100 mL acrylonitrile waste diluted to 500 mg L^{-1}, 200 mg catalyst and 8 mL H_2O_2 (30% wt) were put into a round bottom flask, and the mixture were fully stirred in dark room for 30 minutes. The photo-CWPO degradation process was carried out under the irradiation of high pressure sodium lamp (λ = 589.3 nm, 400 W) for 60 min and keeping the water bath temperature 40 °C. After that, the mixture was separated by centrifugation. The concentration of COD was determined by rapid digestion spectrophotometry (HJ/T399-2007) and the COD removal was calculated. COD concentration was determined by formula (1).

$$\eta/\% = [(\rho_0 - \rho)/\rho_0] \times 100 \quad (1)$$

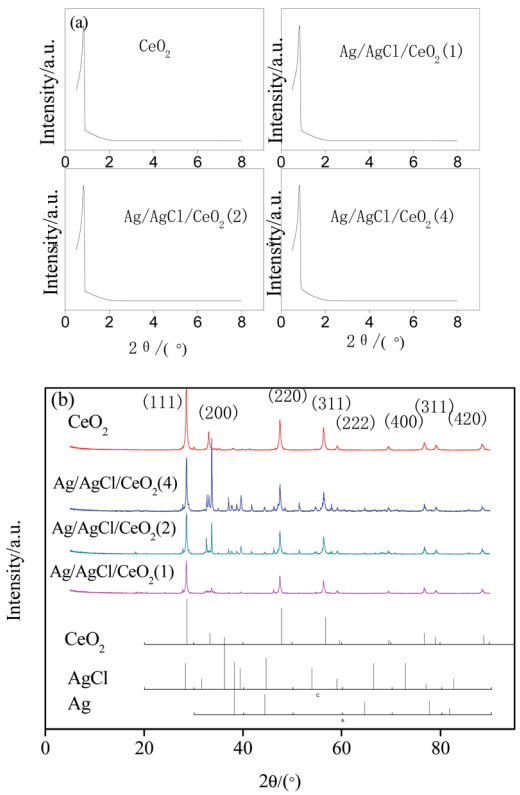

Fig. 1 XRD patterns of samples (a) small-angle diffraction pattern (b) wide-angle diffraction pattern.

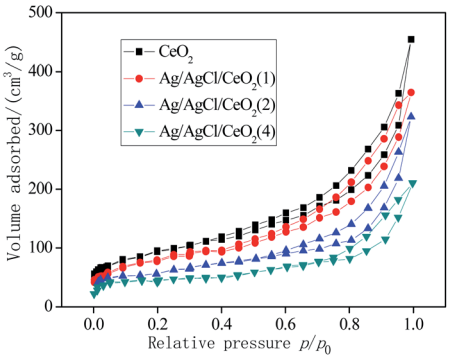

Fig. 2 N_2 adsorption–desorption isotherms of samples.

where: η is the COD removal (%); ρ_0 is the initial concentration of COD (mg L^{-1}); ρ is the COD concentration in the solution after catalytic reaction (mg L^{-1}).

Results and discussion

Catalyst characterization

X-ray diffraction analysis. The structure and composition of various synthesized Ag/AgCl/CeO_2(x) catalysts were studied by X-ray diffraction (XRD) patterns. As shown in Fig. 1a, the small angle diffraction pattern of the samples form sharp peaks near 0.5°(2θ), this indicates that the samples have good crystallinity and ordered mesoporous structure. The loading of Ag does not change the mesoporous structure of CeO_2.[25] From Fig. 1b, compared with the characteristic diffraction peaks of Ag (JCPDS no. 65-2871), AgCl (JCPDS no. 31-1238) and CeO_2 (JCPDS no. 34-0394), the wide angle diffraction pattern shows that the CeO_2 has face centered cubic structure.[26,27] The characteristic peaks of Ag and AgCl appear on the spectra of Ag/AgCl/CeO_2(x), which indicates that the cubic phase AgCl crystals are formed on the surface of CeO_2 under the irradiation of high pressure sodium lamp, and some Ag^+ in AgCl are reduced to Ag atoms, which are aggregated to form cubic Ag and deposited on the surface of AgCl particles. Also, with the increase of Ag doping amount, the characteristic peak intensity of Ag increases.

N_2 adsorption–desorption analysis. The N_2 adsorption–desorption isotherm of the samples are exhibited in Fig. 2. The isotherms belong to IV isotherms according to the IUPAC classification, which are typical cage structure characteristics, indicating that the loaded samples have mesoporous structure. There is an obvious H2 type hysteresis in the range of P/P_0 between 0.6 and 0.9, which indicates that Ag and AgCl are successfully loaded on CeO_2 without changing the original mesoporous structure of CeO_2.[28] The structure parameters of the samples are shown in Table 1. The pore size and the specific surface area range of Ag/AgCl/CeO_2(x) are 8.04–8.90 nm and 302.6–336.2 m^2 g^{-1}. All of them are less than

Table 1 Structural property of the catalysts

Catalysts	Pore size/nm	Pore volume/(cm^3 g^{-1})	Specific surface area/(m^2 g^{-1})
CeO_2	9.06	0.67	350.1
Ag/AgCl/CeO_2(1)	8.90	0.50	336.2
Ag/AgCl/CeO_2(2)	8.82	0.34	317.5
Ag/AgCl/CeO_2(4)	8.04	0.31	302.6

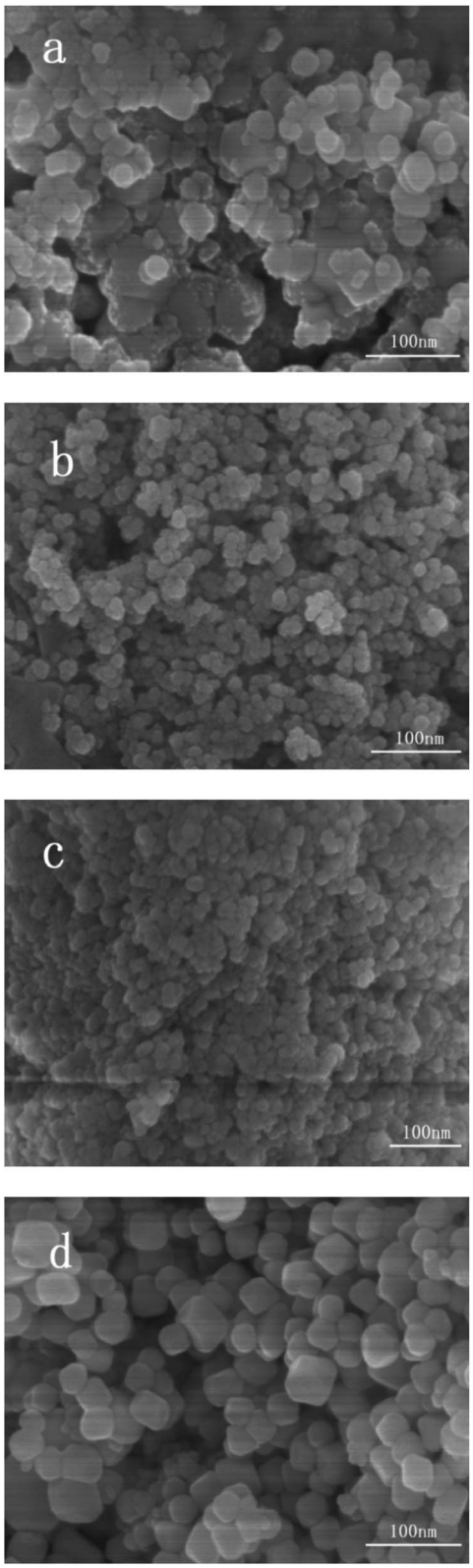

Fig. 3 SEM images of samples (a) Ag/AgCl/CeO_2(1); (b) Ag/AgCl/CeO_2(2); (c) Ag/AgCl/CeO_2(4); (d) CeO_2.

that of CeO_2. Compared with CeO_2, the pore structure of Ag/AgCl/CeO_2(x) samples changed significantly, which may be due to the redox reaction of Ag^+–Ag^0.[29] By comparing the pore structure parameters of these catalysts, it was found that with the increase of Ag doping, Ag accumulated and blocked in the pores, resulting in the decrease of S_{BET} and V_p values.

In general, CeO_2 and Ag/AgCl/CeO_2 synthesized by microwave-assisted soft template have large specific surface area and relatively large pore size, which are conducive to deal with large molecules or groups in the catalytic reactions.[30]

Microstructural analysis. To observe the surface morphology and composition of Ag/AgCl/CeO_2(x), the catalysts were scanned by SEM. It can be seen from the SEM image (Fig. 3a) that CeO_2 are cubic particles and stack into porous structure. Ag and AgCl nanoparticles dispers well on the surface of CeO_2. With the increase of Ag loading, the particle size of Ag and AgCl decrease and the accumulation become more dense (Fig. 3b–d).

EDS analysis was carried out under scanning electron microscope to determine the composition and spatial distribution of the constituent elements of the sample. As shown in Fig. 4, there are Ce, O, Ag and Cl in the samples. The distribution of various elements are very uniform, and the ratio of Ag to Cl in Ag/AgCl/CeO_2(x) samples is greater than 1, which further confirmed the existence of silver. EDS content analysis of each element are shown in Table 2. According to Table 2, with the amount of $AgNO_3$ increased sequentially, the content of Ag in the samples increased sequentially.

The TEM images are shown in Fig. 5, which indicates that CeO_2 prepared has ordered mesoporous structure with clear lattice fringes. Ag and AgCl particles are formed on the surface of CeO_2. This result is consistent with that of N_2 adsorption–desorption test.

Ultraviolet visible spectrum analysis. Fig. 6 shows the UV-Vis DRS spectra and band gap of CeO_2 and Ag/AgCl/CeO_2(x). Fig. 6a is the UV-Vis DRS spectra which shows that CeO_2 and Ag/AgCl/CeO_2(x) exhibit strong absorption in the ultraviolet region (200 nm < λ < 400 nm), while CeO_2 exhibits weak absorption in the 400–450 nm visible region. However, Ag/AgCl/CeO_2(x) has strong absorption in the visible region of 400–700 nm. It is due to the effective surface plasmon resonance of Ag nanoparticles, which can significantly improve the absorption of photocatalyst in the visible region.[31,32] As can be seen from Fig. 6b, the band gap of CeO_2 is 3.1 eV, while the band gap of Ag/AgCl/CeO_2(2) reduces to 2.9 eV, so that photons with longer wavelength and lower energy can be excited, the absorption spectrum is red shifted, the utilization rate of photons is improved, and the catalytic efficiency is improved. However, the excessive Ag decoration on the surface of CeO_2 particles increases the distance of photogenerated electrons and holes from the inside to the surface and the recombination probability.[33] The formation of Ag nanoparticles on Ag/AgCl/CeO_2(x) catalyst is further confirmed, and the absorption intensity is related to the amount of Ag doping.

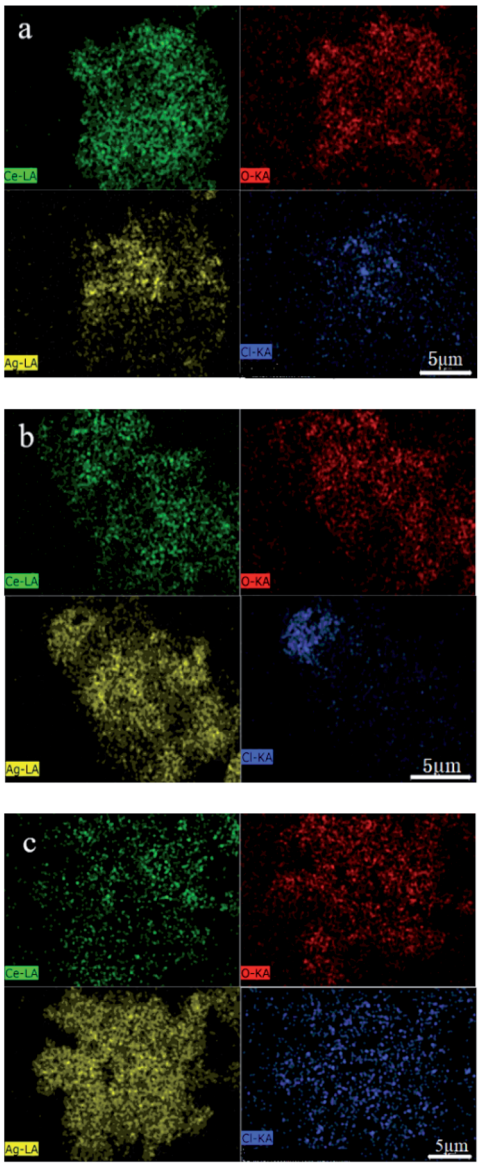

Fig. 4 Element distribution images of samples: (a) Ag/AgCl/CeO_2(1); (b) Ag/AgCl/CeO_2(2); (c) Ag/AgCl/CeO_2(4).

Catalytic performance

Catalytic performance in different reaction systems. Different experimental systems were set up to compare the catalytic performance, namely (a) visible light + CWPO; (b) CWPO; (c) visible light catalysis; (d) visible light + H_2O_2; (e) CeO_2 + H_2O_2. The results are shown in Fig. 7. It can be seen from Fig. 7 that the COD removal trend of each system is (a) > (b) > (e) > (c) > (d).

The COD removal of system (d) is the lowest, indicating that the catalytic degradation efficiency of organic matter is the

Table 2 EDS analysis of element mass fraction

	Atomic percentage of elements (%)			
Samples	Ag	Cl	Ce	O
Ag/AgCl/CeO_2(1)	20.19	17.02	22.48	40.31
Ag/AgCl/CeO_2(2)	28.74	20.28	19.14	31.84
Ag/AgCl/CeO_2(4)	33.26	23.09	15.87	27.78

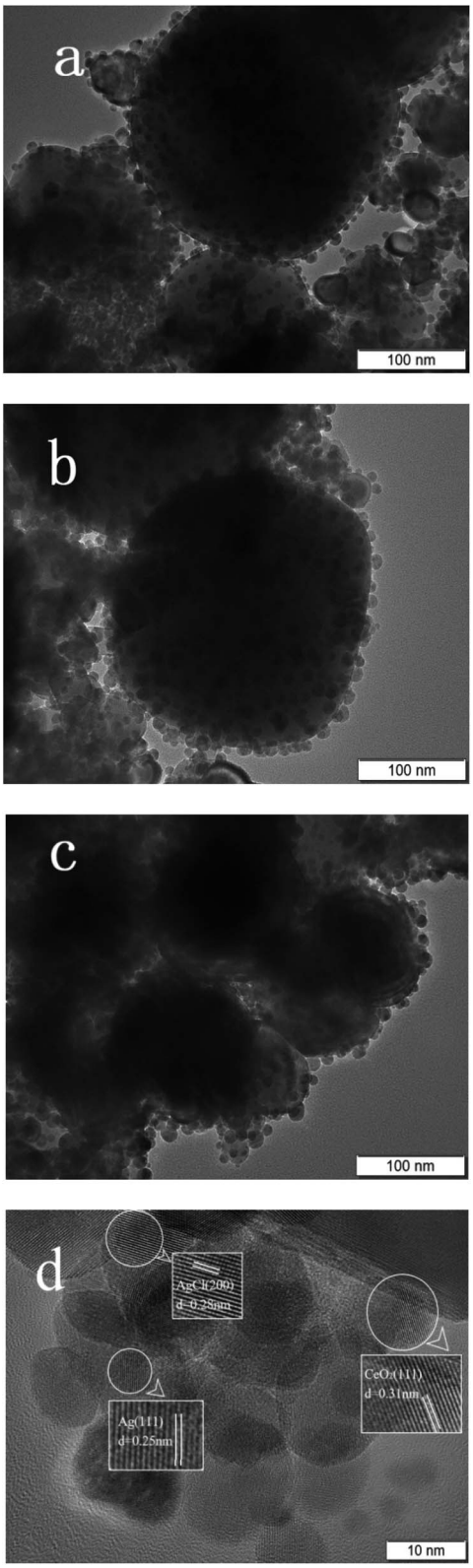

Fig. 5 TEM images of samples: (a) Ag/AgCl/CeO_2(1); (b) Ag/AgCl/CeO_2(2); (c) Ag/AgCl/CeO_2(4); (d) CeO_2.

lowest. That's because only H_2O_2 is added as oxidant in system (d), and the oxidation potential of H_2O_2 is 1.78 eV, while the oxidation potential of ˙OH is 2.8 eV.[34] Therefore, the

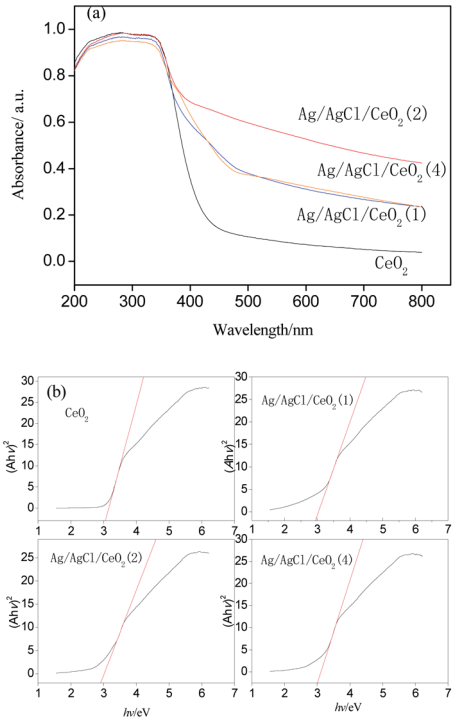

Fig. 6 UV-Vis diffuse-reflectance spectra of catalysts (a) and their band gap (b).

oxidizability of H_2O_2 is weaker than that of ˙OH. The irradiation of visible light can not make H_2O_2 produce enough ˙OH, moreover, visible light can decompose H_2O_2 into H_2O and O_2, which reduces the utilization of H_2O_2 and leads to the worst COD removal.[2,35]

System (c) is a typical photocatalytic reaction, which proved that Ag/AgCl/CeO_2(2) can effectively absorb visible light and has good photocatalytic activity. Because visible light can excite Ag/AgCl and CeO_2 to produce photogenerated electron e^- and photogenerated hole h^+, which can oxidize H_2O around the catalyst to generate ˙OH due to its strong oxidizability. e^- and h^+ can also oxidize Cl^- in AgCl to produce active species Cl^0 with

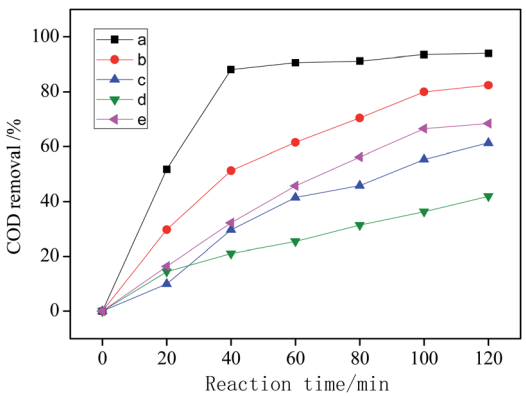

Fig. 7 COD removal under different conditions: (a) visible light + CWPO; (b) CWPO; (c) visible light catalysis; (d) visible light + H_2O_2; (e) CeO_2 + H_2O_2.

oxidation, and even directly participate in the catalytic degradation of organic pollutants.

System (b) and system (e) are wet catalytic oxidation reactions with different catalysts. CeO_2/H_2O_2 has the cycle of Ce^{3+}/Ce^{4+}, which promoted the decomposition of H_2O_2 into $^{\cdot}OH$ and $^{\cdot}O^{2-}$.[36] Noble metal Ag supported on the surface of CeO_2 can increase the lattice oxygen defects of CeO_2 and improve its catalytic performance.[37] Compared with system (e), the catalytic performance of CeO_2 can be improved by loading Ag and AgCl.

System (a) shows that $Ag/AgCl/CeO_2(2)$ has the best catalytic performance in the photo-CWPO system, it is proved that synergistic effects of various active species mentioned above improved the catalytic performance of $Ag/AgCl/CeO_2$ and the COD removal reaches 90% in 60 min.

Effect of catalyst dosage and Ag loading on catalytic performance. In the catalytic performance tests, the initial concentration of COD is 500 mg L^{-1}, 8 mL H_2O_2 (30% wt), water bath temperature 40 °C, irradiation of high pressure sodium lamp (λ = 589.3 nm, 400 W) for 60 min. The dosage of $Ag/AgCl/CeO_2(2)$ was separately changed into 50 mg, 100 mg, 200 mg and 400 mg to investigate the effect of catalyst dosage on COD removal. The results are shown in Fig. 8. With the increase of catalyst dosage from 50 mg to 200 mg, the COD removal increases, and the maximum COD removal reaches 90% when the catalyst dosage is 200 mg; continue to increase the dosage of catalyst, the COD removal decreases slightly. This is due to the increase of particle contact opportunities, the appearance of particle agglomeration, the decrease of active centers in contact with organic matter, resulting in the decrease of utilization of $^{\cdot}OH$ in the degradation of organic matter molecules.[38]

The Ag ion doped is an effective electron receiver, which can capture the electrons in the conduction band. The competition of metal ions for electrons makes the photogenerated electron e^- and photogenerated hole h^+ separate, which reduce the recombination probability of the e^- and h^+ on CeO_2 surface, so that more $^{\cdot}OH$ can be produced on CeO_2 surface under the action of visible light radiation and improve the catalytic activity.[39]

At lower Ag loading (1 mmol), Ag particles enter into the deep pores of CeO_2 and can not participate in the catalytic peroxidation reaction. Only some Ag particles at the opening of the pores participated in the oxidation reaction. There are not enough active sites on the surface of the catalyst, which lead to the lower efficiency of the catalyst. With the increase of Ag loading to 2 mmol, the $Ag/AgCl/CeO_2$ catalyst has higher catalytic activity and the COD removal reach 90%. When Ag loading is further increased to 4 mmol, Ag becomes the center of fast recombination of electrons and holes, and the catalytic activity decreases.[40,41] Moreover, the size of $Ag/AgCl/CeO_2$ decreases and aggregates are formed. These aggregated particles are heavy and high density, resulting in the decrease of the surface active center and the decrease of COD removal.

Effect of H_2O_2 dosage on catalytic performance. In the photo-CWPO system, H_2O_2 plays an important role in the degradation of organic compounds. The formation of $^{\cdot}OH$ mainly depends on the content of H_2O_2 in the solution. In the catalytic performance test, the initial concentration of COD is 500 mg L^{-1}, 200 mg catalyst water bath temperature 40 °C, irradiation of high pressure sodium lamp (λ = 589.3 nm, 400 W) for 60 min. The dosage of H_2O_2 (30% wt) was separately changed into 2 mL, 4 mL, 6 mL, 8 mL and 10 mL. The effect of H_2O_2 dosage on COD removal was investigated. The results are shown in Fig. 9. It can be seen from Fig. 9 that the COD removal increase with the increase of H_2O_2 dosage, and the maximum COD removal is 84.12% at 8 mL. When the dosage of H_2O_2 is 10 mL, the COD removal decreases slightly. This is because excessive H_2O_2 can lead to the consumption of $^{\cdot}OH$ itself and convert it to hydroxyl radical ($^{\cdot}HO_2^-$).[42,43] The ineffective decomposition of H_2O_2 leads to a decrease in $^{\cdot}OH$ production.

Effect of pH value on catalytic performance. The effect of pH on the catalytic degradation of organic compounds was investigated by adjusting the solution pH at 4, 5, 6, 7, 8 and 9 with HCl or NaOH solution. It can be seen from Fig. 10 that when pH value increased from 4 to 6, the COD removal increases. When pH value is higher than 6, the COD removal decreases obviously. That is because the potential of $^{\cdot}OH$ is higher when the pH value is 6. Organic molecules undergo protonation or deprotonation in alkaline or acidic media. When pH < 6, due to electrostatic repulsion, organic molecules protonated, and the interaction with $Ag/AgCl/CeO_2$ active center is poor. Under alkaline conditions, H_2O_2 decomposes into H_2O and O_2 on the

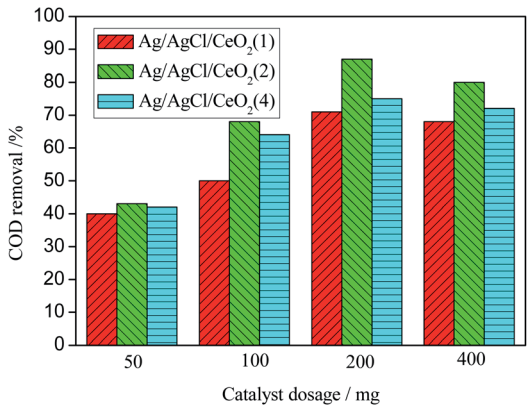

Fig. 8 Effect of catalyst dosage and Ag loading on COD removal.

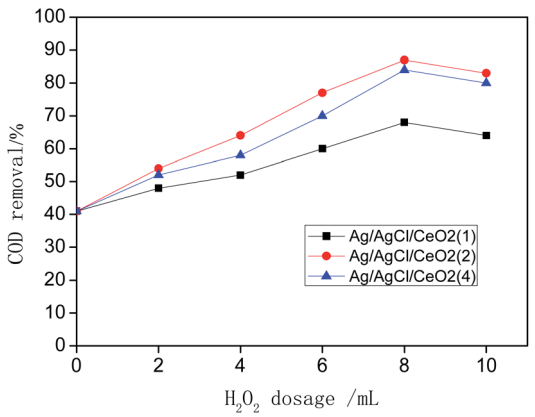

Fig. 9 The effect of H_2O_2 on COD removal.

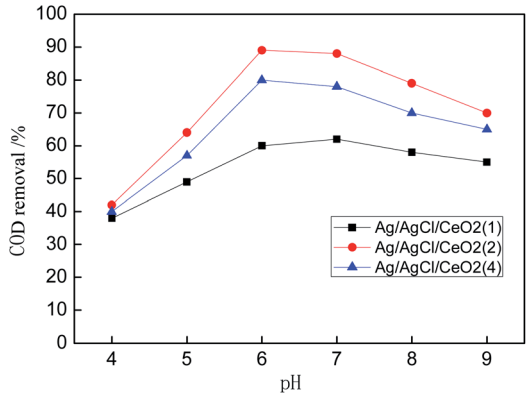

Fig. 10 The effect of pH on COD removal.

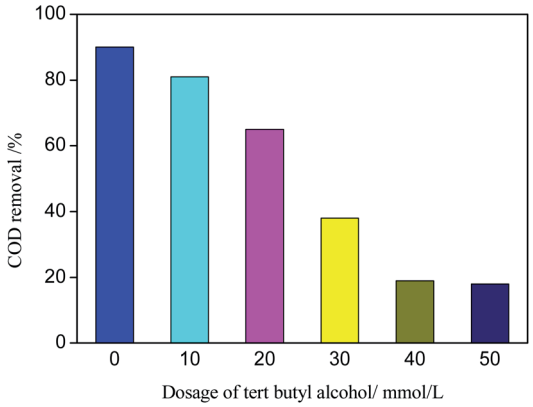

Fig. 12 Effect of *tert*-butyl alcohol on COD removal.

surface of the catalyst. Moreover, the alkaline solution neutralizes the charge on the catalyst surface, thereby reducing the activity of the catalyst.[44,45] Therefore, the optimal pH value of Ag/AgCl/CeO_2 in photo-CWPO system is 6. In this experiment, the initial pH of experimental wastewater is 6, so it is no need to adjust the pH of acrylonitrile wastewater.

Reusability

During the development of CWPO technology, the stability of catalyst is of great significance to its practical application. Fig. 11 shows the catalytic degradation effect of Ag/AgCl/CeO_2(2) on organic matter for 5 times. The COD removal decreases slightly after each operation, but the catalyst still has more efficient activity. The COD removal is about 85% after the 5th reaction. The results show that Ag/AgCl/CeO_2 has good stability and can be reused.

Mechanism exploration

tert-Butyl alcohol is the scavenger of ˙OH.[46] Different amounts of *tert*-butyl alcohol were added to the catalytic performance tests to verify the reaction mechanism of ˙OH chain formed in the degradation process of organic matter in photo-CWPO system. The effect of *tert*-butyl alcohol dosage on COD removal is shown in Fig. 12. According to Fig. 12, with the increase of *tert*-butyl alcohol amount, the COD removal decreases obviously. When the *tert*-butyl alcohol amount is 40 mmol L^{-1}, the COD removal is 19%. Continue to increase the *tert*-butyl alcohol amount, the COD removal changes slightly. It is due to that ˙OH is more easily captured by *tert*-butyl alcohol during the competition with organics, almost all the generated ˙OH is captured by *tert*-butyl alcohol and generated inert substances, which inhibited the oxidative degradation of organics. When the amount of *tert*-butyl alcohol continues to increase, the COD removal remains at 19%, it is because active species such as h^+, $\cdot O_2^-$ and Cl^0 in photo-CWPO system can also oxidize organic pollutants.[47] Meanwhile, it also indicates that ˙OH plays a major role in the degradation process of organic matter.

In the photo-CWPO system, the degradation of organic compounds can be attributed to both Ag/AgCl plasma resonance and Ce^{3+}/Ce^{4+} cycling. According to the mechanism of plasma photocatalysis of Ag@AgCl[18] and the Fenton like mechanism of CeO_2/H_2O_2,[48] the reaction mechanism of Ag/AgCl/CeO_2 in photo-CWPO system can be summarized as the following steps and as shown in Fig. 13. First of all, under visible light irradiation, due to the plasma resonance effect of

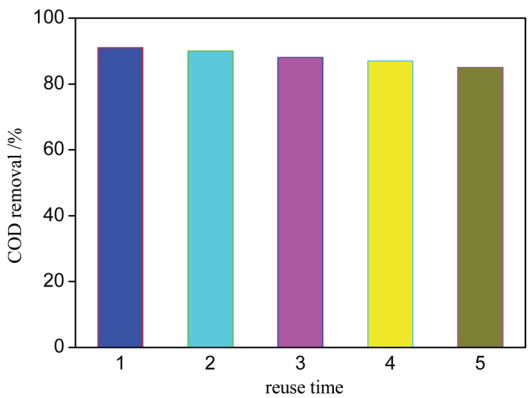

Fig. 11 Effect of catalyst reuse time on COD removal.

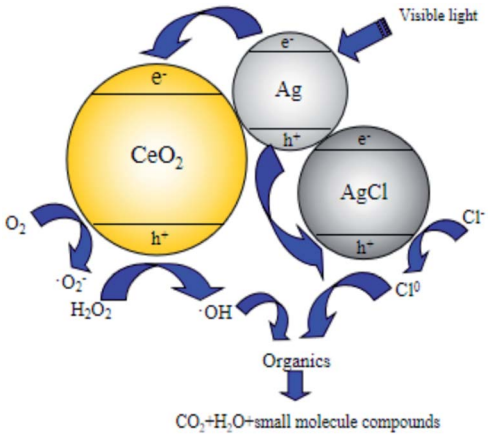

Fig. 13 Mechanism of acrylonitrile wastewater degradation in photo-CWPO process.

Ag nanoparticles, it is easy to absorb visible light and produce photogenerated electron e^- and hole h^+. CeO_2 has excellent dielectric transfer ability under visible light, which helps to improve its charge separation ability.[49,50] Photogenerated electron e^- is injected into the 4f band of CeO_2 and trapped by oxygen on the CeO_2 surface to form superoxide radicals ($^{\bullet}O_2^-$), then form H_2O_2, hydroperoxyl (HO_2^-) and $^{\bullet}OH$. When the hole h^+ is transferred to the surface of AgCl, another active radical species Cl^0 is formed, which can oxidized the organic matter and reduced to Cl^-. Therefore, through the synergistic effect of various active species in the photo-CWPO system, and these processes are stable and cyclic, so that organic pollutants can be effectively degraded.[51]

Conclusions

In this paper, silver/silver halide supported on mesoporous ceria particles (Ag/AgCl/CeO_2) was successfully prepared using microwave assisted soft template method, deposition precipitation method and photoreduction method. The specific surface area of Ag/AgCl/CeO_2 is 302.6–336.2 $m^2\ g^{-1}$ and average pore size is 8.04–8.90 nm. The catalytic performance test showed that the Ag/AgCl has signifificantly improved the catalytic performance of CeO_2 in photo-CWPO under visible light system. According to the experimental data, the COD removal of acrylonitrile wastewater reach 90%, and after the catalyst was used for 5 times, the COD removal can still reach 85% by using Ag/AgCl/CeO_2(2) as catalyst under the optimum reaction condition. In addition, the synergistic effect of Ag, AgCl, CeO_2 and H_2O_2 in photo-CWPO system were also observed. It is proved that $^{\bullet}OH$ plays a major role in the degradation of organic matter in the photo-CWPO system.

Conflicts of interest

The authors declare that they have no conflict of interest.

Acknowledgements

The project was funded by National Water Pollution Control and Management Technology Major Projects (2012ZX07202-002); Science and Technology Research Project of Liaoning Provincial Department of Education (L2020020, L2020003).

References

1 A. Kumar and B. Prasad, *Int. J. Environ. Sci. Technol.*, 2020, **17**(3), 1809–1824.
2 H. H. Fenton, *J. Chem. Soc., Trans.*, 1894, **65**, 899–910.
3 Tu, Y. Pan, H. J. Gao, B. Li and Y. H. Song, *Environ. Sci. Pollut. Res.*, 2019, **26**(24), 1–11.
4 B. Wang and G. L. Jing, *Recent Pat. Chem. Eng.*, 2013, **6**(2), 127–132.
5 A. Kumar, B. Prasad, V. K. Sandhwar and K. K. Garg, *J. Environ. Chem. Eng.*, 2021, **9**(3), 105177.
6 Y. Hu, Y. Li, J. He, T. Liu, K. S. Zhang and X. J. Huang, *J. Environ. Manage.*, 2018, **226**(15), 256–263.
7 H. Li, R. Cheng, Z. Liu and C. Du, *Sci. Total Environ.*, 2019, **683**(5), 638–647.
8 X. Hu, R. Li, S. Zhao and Y. Xing, *Appl. Surf. Sci.*, 2017, **396**, 1393–1402.
9 Z. Wan and J. Wang, *Environ. Sci. Pollut. Res.*, 2017, **396**(28), 1393–1402.
10 A. El Gaidoumi, J. M. Dona-Rodriguez, E. Pulido Melian, O. M. Gonzalez-Diaz, J. A. Navio and B. El Bali, *Arabian J. Sci. Eng.*, 2019, **44**(7), 6313–6325.
11 W. Long, W. Tong, W. Han and J. Zhong, *Prog. Nat. Sci.*, 2018, **28**(1), 24–27.
12 B. Son, V. Q. Mai and D. X. Du, *J. Porous Mater.*, 2016, **24**(3), 601–611.
13 Z. P. Li, F. Liu, Y. Ding, F. Wang, H. You and C. Jin, *Chemosphere*, 2019, **214**(11), 17–24.
14 A. Hassani, G. Celikdag and P. Eghbali, *Ultrason. Sonochem.*, 2018, **40**(A), 841–852.
15 P. G. Munoz, G. Pliego, J. A. Zazo, B. Barbero, A. Bahamonde and J. A. Casas, *Chem. Eng. J.*, 2016, **318**(15), 89–94.
16 A. O. Ifelebuegu, J. Ukpebor and B. Nzeribe-Nwedo, *Int. J. Environ. Sci. Technol.*, 2016, **13**(12), 2757–2766.
17 M. Golestanbagh, M. Parvini and A. Pendashteh, *Catal. Lett.*, 2018, **148**(7), 2162–2178.
18 P. Wang, B. B. Huang and X. Y. Qin, *Angew. Chem., Int. Ed.*, 2008, **47**(41), 7773–7965.
19 M. Wu, L. Yan, J. Li and L. Wang, *Res. Chem. Intermed.*, 2017, **43**(11), 6407–6419.
20 J. Zhang, C. G. Niu, J. Ke, L. F. Zhou and G. M. Zeng, *Catal. Commun.*, 2015, **59**, 30–34.
21 X. Guan, S. Lin, J. Lan, J. Shang and Q. Song, *Cellulose*, 2019, **26**(12), 7437–7450.
22 F. Mu, C. Liu, Y. Xie, S. Zhou and D. Y. C. Leung, *Chem. Eng. J.*, 2021, **415**(6), 129010.
23 C. Gfab, A. Rn, A. Zy, L. D. Jing and A. Bd, *J. Hazard. Mater.*, 2020, **403**, 123964.
24 N. Su and F. Zhou, *React. Kinet., Mech. Catal.*, 2020, **129**(2), 1077–1089.
25 M. Chernykh, N. Mikheeva, V. Zaikovskii, M. Salaev and G. Mamontov, *Catalysts*, 2020, **10**(5), 580–592.
26 B. Matovic, S. Butulija, Z. Dohcevic-Mitrovic, T. Arsic, J. Lukovic and S. Boskovic, *J. Eur. Ceram. Soc.*, 2020, **40**(5), 1983–1988.
27 M. M. Khan and S. A. Ansari, *Ind. Eng. Chem. Res.*, 2014, **53**(23), 9754–9763.
28 P. J. Brewer, A. S. Leach and R. Brown, *Electrochim. Acta*, 2015, **161**, 80–83.
29 L. Yang, F. Wang, C. Shu, P. Liu, W. Zhang and S. Hu, *Sci. Rep.*, 2016, **6**, 21617.
30 D. Y. Zhao, Q. S. Huo, J. G. Feng, F. B. Chmelka and G. D. Stucky, *J. Am. Chem. Soc.*, 1998, **120**(24), 6024–6036.
31 K. Awazu, M. Fujimaki, C. Rockstuhl, J. Tominaga, H. Murakami and Y. Ohki, *J. Am. Chem. Soc.*, 2008, **130**(5), 1676–1680.
32 X. Chen, H. Zhu, J. Zhao, Z. Zheng and X. Gao, *Angew. Chem.*, 2008, **47**(29), 5353–5356.
33 A. Di, Y. Wang and G. Chen, *Funct. Mater. Lett.*, 2018, **11**(1), 1850006.1–1850006.4.

34 M. Chernykh, N. Mikheeva, V. Zaikovskii, M. Salaev and G. Mamontov, *Catalysts*, 2020, **10**(5), 580–591.
35 E. G. Heckert, S. Seal and W. T. Self, *Environ. Sci. Technol.*, 2008, **42**(13), 5014–5019.
36 S. J. Wu, Y. Yang, C. X. Lu, Y. Y. Ma, S. X. Yuan and G. R. Qian, *Eur. J. Inorg. Chem.*, 2018, **25**, 2944–2951.
37 S. Q. Wang, H. Li and M. Wu, *J. Cleaner Prod.*, 2021, **303**, 126825.
38 B. Yadav and V. C. Srivastava, *Clean Technol. Environ. Policy*, 2017, **19**(5), 1547–1555.
39 X. J. Wen, C. G. Niu, D. W. Huang, L. Zhang, C. Liang and G. M. Zeng, *J. Catal.*, 2017, **355**, 73–86.
40 V. Subbaramaiah, V. C. Srivastava and I. D. Mall, *J. Hazard. Mater.*, 2013, **248–249**(15), 355–363.
41 P. Mohammad, A. Seyed, A. Hamidreza and R. Mehran, *Catalysts*, 2018, **8**(9), 388–399.
42 X. M. Guan, Y. F. Zhan, L. Yang, J. W. Lan and S. Lin, *Cellulose*, 2020, **27**(11), 6383–6398.
43 L. G. Devi, S. G. Kumar, K. M. Reddy and C. Munikrishnappa, *J. Hazard. Mater.*, 2009, **164**(2–3), 459–467.
44 M. M. Ahmed and S. Chiron, *Water Res.*, 2014, **48**(1), 229–236.
45 S. Singh and S.-L. Lo, *Chem. Eng. J.*, 2017, **309**(1), 753–765.
46 H. Yan, R. Wang, R. X. Liu, T. Xu and J. Wang, *Appl. Catal., B*, 2021, **291**(8), 120096.
47 Y. Baba, T. Yatagai, T. Harada and Y. Kawase, *Chem. Eng. J.*, 2015, **277**(1), 229–241.
48 E. G. Heckert, S. Seal and W. T. Self, *Environ. Sci. Technol.*, 2008, **42**(13), 5014–5019.
49 Y. Zou, H. Huang, S. Li, J. Wang and Y. Zhang, *J. Photochem. Photobiol., A*, 2019, **376**, 43–53.
50 C. G. Li, L. H. Yue, J. J. Wang, H. Zhou, R. Zhang and K. Li, *Environ. Technol.*, 2021, **22**(1), 1–16.
51 V. Gosu, S. Arora and V. Subbaramaiah, *Environmental Engineering Research*, 2019, **25**(4), 488–497.